How to cite: *Angew. Chem. Int. Ed.* **2021**, *60*, 9032–9037
International Edition: doi.org/10.1002/anie.202100172
German Edition: doi.org/10.1002/ange.202100172

Gas Separation

High-Silica CHA Zeolite Membrane with Ultra-High Selectivity and Irradiation Stability for Krypton/Xenon Separation

Xuerui Wang[+], Tao Zhou[+], Ping Zhang, Wenfu Yan, Yongguo Li, Li Peng, Dylan Veerman, Mengyang Shi, Xuehong Gu,* and Freek Kapteijn**

Abstract: *Capture and storage of the long-lived ^{85}Kr is an efficient approach to mitigate the emission of volatile radionuclides from the spent nuclear fuel reprocessing facilities. However, it is challenging to separate krypton (Kr) from xenon (Xe) because of the chemical inertness and similar physical properties. Herein we prepared high-silica CHA zeolite membranes with ultra-high selectivity and irradiation stability for Kr/Xe separation. The suitable aperture size and rigid framework endures the membrane a strong size-exclusion effect. The ultrahigh selectivity of 51–152 together with the Kr permeance of $0.7–1.3\times10^{-8}\,mol\,m^{-2}\,s^{-1}\,Pa^{-1}$ of high-silica CHA zeolite membranes far surpass the state-of-the-art polymeric membranes. The membrane is among the most stable polycrystalline membranes for separation of humid Kr/Xe mixtures. Together with the excellent irradiation stability, high-silica CHA zeolite membranes pave the way to separate radioactive Kr from Xe for a notable reduction of the volatile nuclear waste storage volume.*

Introduction

Nuclear power plants supplied in 2017 about 10% of the world's electricity, 2636 TWh, avoiding 2388 million tonnes of annual CO_2 emission from power plants fired by natural gas—by far the cleanest burning fossil fuel.[1] However, the spent nuclear fuel is highly radioactive and must be carefully reprocessed to recover plutonium and uranium for advanced fuel cycles and to safeguard human health and minimize the impact on the environment.[2] Volatile radionuclides, predominately Kr and Xe generated during irradiation of the fuel, are released into the reprocessing off-gas streams and ultimately into the environment. The only significant reduction of ^{85}Kr is by radioactive decay with a long half-life of 10.76 years. For this reason the emitted ^{85}Kr has accumulated in the atmosphere, causing a fifteen-fold increase in radioactivity concentration from $0.1\,Bq\,m^{-3}$ in 1959 to current $1.45\,Bq\,m^{-3}$ in Central Europe.[3] The ^{85}Kr intensifies the ionization of atmospheric gases and results in irreversible climate changes.[4] Therefore, the capture and storage of ^{85}Kr from off-gases came into the focus.

The separation of Kr from Xe is highly challenging but economically attractive due to a ten-fold volume reduction for radioactive ^{85}Kr storage. Cryogenic distillation is technically feasible but energy intensive due to the operation at low temperature and high pressure.[5] Physical adsorption based on activated carbon,[6] zeolites,[6,7] metal-organic frameworks,[8] porous organic frameworks[9] is deemed an energy-efficient alternative that can be operated at near-ambient conditions. However, the adsorbents are generally Xe selective over Kr due to the stronger Van der Waals' interactions (thermodynamic control).[10] Considering the lower abundancy of Kr (Kr/Xe ratio = 9/91), a selective adsorption of Kr over Xe (kinetic control) is preferred to improve the economic feasibility, whereas this kind of adsorbent is rarely explored.[11]

To enhance the Kr-selective adsorption, Thallapally and co-workers pioneered a dual-bed cascade system, including a Xe selective adsorbent bed followed by Kr adsorption in the second bed.[12] Alternatively, kinetic control (diffusion selectivity) can easily dominate over thermodynamic control in membrane gas separation, evidenced by the separation of H_2/CO_2,[13] N_2/CH_4[14] and CO_2/Xe.[15] However, Kr/Xe membrane separation is challenging because the kinetic diameter difference between Kr (0.36 nm) and Xe (0.396 nm) is less

[*] Prof. Dr. X. Wang,[+] T. Zhou,[+] P. Zhang, Dr. L. Peng, M. Shi, Prof. Dr. X. Gu
State Key Laboratory of Materials-Oriented Chemical Engineering, College of Chemical Engineering, Jiangsu National Synergetic Innovation Center for Advanced Materials, Nanjing Tech University
No. 30 Puzhu South Road, Nanjing 211816 (P. R. China)
E-mail: x.wang@njtech.edu.cn
xhgu@njtech.edu.cn

D. Veerman, Prof. Dr. F. Kapteijn
Chemical Engineering Department, Delft University of Technology
Van der Maasweg 9, 2629 HZ Delft (The Netherlands)
E-mail: f.kapteijn@tudelft.nl

Prof. Dr. W. Yan
State Key Laboratory of Inorganic Synthesis and Preparative Chemistry, College of Chemistry, Jilin University
Changchun 130012 (P. R. China)

Dr. Y. Li
Environment Engineering Department, China Institute for Radiation Protection, Taiyuan 030006 (P. R. China)

[+] These authors contributed equally to this work.

Supporting information and the ORCID identification number(s) for the author(s) of this article can be found under https://doi.org/10.1002/anie.202100172.

than 0.04 nm and Xe is preferentially adsorbed over Kr (competitive adsorption control). Polycrystalline membranes featuring a well-defined pore structure are the most promising for Kr/Xe separation in view of working capacity (permeance) and efficiency (selectivity).[16] The reported polycrystalline membranes for Kr/Xe separation, such as SAPO-34,[16a–d] are extremely sensitive to moisture because channel blockage[17] and framework collapse[18] occurred through water uptake from off-gas streams.[19] Sufficient resistance to γ-radiation is another essential criterion for practical application using radioactive ^{85}Kr,[12a] but the radiation stability of polycrystalline membranes is hardly reported.[20]

Herein we prepared high-silica CHA zeolite membranes on ceramic hollow fiber substrates for Kr/Xe separation. The elliptical pore opening of high-silica CHA zeolite is 0.370 × 0.417 nm,[21] narrower than that of benchmark SAPO-34 (0.38 × 0.38 nm).[22] More importantly, the framework is less flexible,[23] therefore, a stronger size-exclusion of Kr and Xe atoms is highly anticipated for high-silica CHA zeolite membranes. The high-silica nature endures superior hydrophobicity so that the structural stability and separation performance is insensitive to water vapor. Together with potential resistance to γ-irradiation, the high-silica CHA zeolite membrane would become a new benchmark for radioactive Kr separation from Xe for a notable decrease in the volatile radionuclides' storage volume.

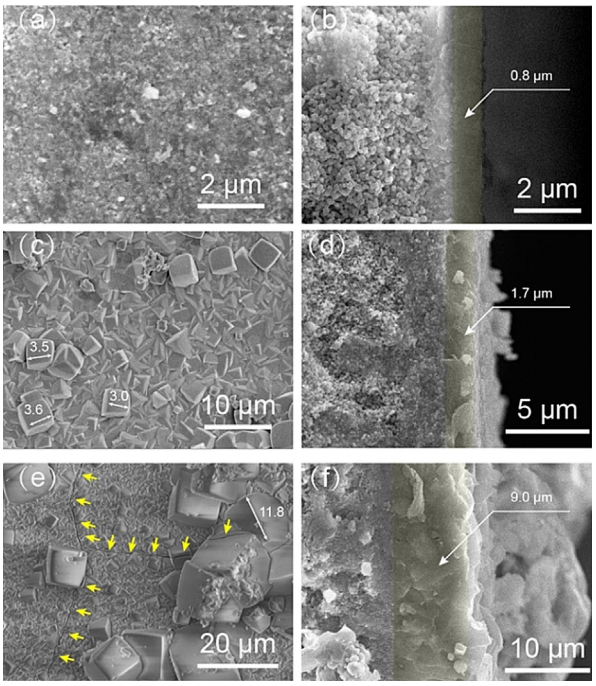

Figure 1. SEM image of high-silica CHA zeolite membranes synthesized for 48 h (a,b), 96 h (c,d) and 144 h (e,f). The temperature was fixed at 433 K and the synthesis composition at 104 SiO_2/1.1 Al_2O_3/10 Na_2O/20 TMAdaOH/4410 H_2O. The well-intergrown layer (right, light yellow marker color) and cracks (left, yellow arrows) are highlighted.

Results and Discussion

The membranes were synthesized by the secondary growth method. Figure 1 shows the representative SEM images of the membranes synthesized for various periods. The porous alumina supports were gradually covered by typical cubic crystals, along with an increasing membrane thickness, as the synthesis time increased. After 48 h synthesis a 0.8-μm-layer formed on the membrane surface without visible cubic morphology (Figure 1 a,b). The thickness increased further to 1.7 μm by prolonging the synthesis time to 96 h (Figure 1 d), which is similar to the one synthesized in fluorine-containing gel by Hedlund and co-workers.[24] Besides the well intergrown layer, few relative large cubic crystals (3.4 ± 0.3 μm) are observed at the surface (Figure 1 c). The convex crystals grow faster than the ones embedded which are more space-confined. Eventually the crystals grew up to 11.8 ± 1.2 μm after hydrothermal synthesis for 144 h (Figure 1 e), similar to the crystals collected from the bottom of autoclave (11.3 ± 1.5 μm, Figure S1). The lower membrane thickness of around 9.0 μm (Figure 1 f) indicates the slower space-confined crystal growth in the membrane layer. The large crystals caused a rough membrane surface, which is unfavorable to the membrane sealing for gas separation.[25] Furthermore, the thickness and uneven grain size caused cracks in the well-intergrown polycrystalline membranes after detemplatation.[26]

The phase composition of the membrane was determined by powder X-ray diffraction (PXRD). The patterns are consistent regardless of synthesis time (Figure S2), confirming the successful synthesis of pure CHA zeolite membranes. The diffraction intensity is enhanced over time as the crystal grains grew and membrane thickness increased. Generally, the silicon species initially aggregate and fuse together to generate zeolitic building blocks covering the parent seeds (induction period). Rimer et al.[27] revealed this period lasted at least 36 h after which high-silica CHA zeolite crystallization was triggered through consuming the amorphous species (growth period). This is the reason why a low diffraction intensity and no cubic crystals are observed after the short synthesis period of 48 h. The amorphous species blocked the pathway for gas transport through the membrane as evidenced by a low Kr permeance of 2.2×10^{-9} mol m^{-2} s^{-1} Pa^{-1} (membrane M1, Table 1). The diffraction intensity remained constant after extending the synthesis time beyond 96 h, indicating a regular zeolitic framework formed.[28] The Kr permeance increased by one order of magnitude and the Kr/Xe mixture selectivity up to 152 (membrane M3).

To obtain the adsorption parameters, single-component isotherms were collected at 273 K, 298 K, 323 K and then

Table 1: Kr/Xe mixture (50/50) separation performance of the membranes synthesized for different periods of time.

Membrane	t [h]	P_{Kr} [mol m^{-2} s^{-1} Pa^{-1}]	$\alpha_{Kr/Xe}$
M1	48	2.2×10^{-9}	26.8
M2	96	1.7×10^{-8}	51
M3	96	1.3×10^{-8}	152
M4	96	7.1×10^{-9}	114
M5	144	7.2×10^{-9}	6.2

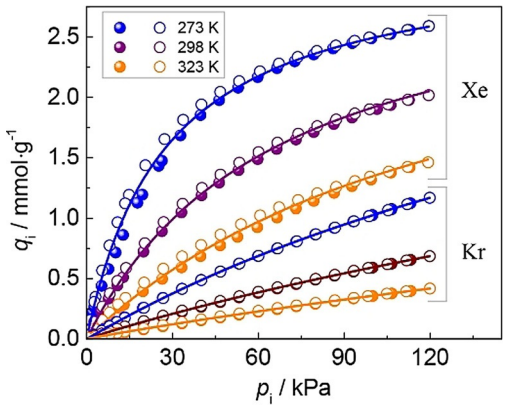

Figure 2. Kr and Xe single-component adsorption isotherms of high-silica CHA zeolite (closed symbols: measured adsorption data points; open symbols: measured desorption data points; line: single-site Langmuir isotherm fit).

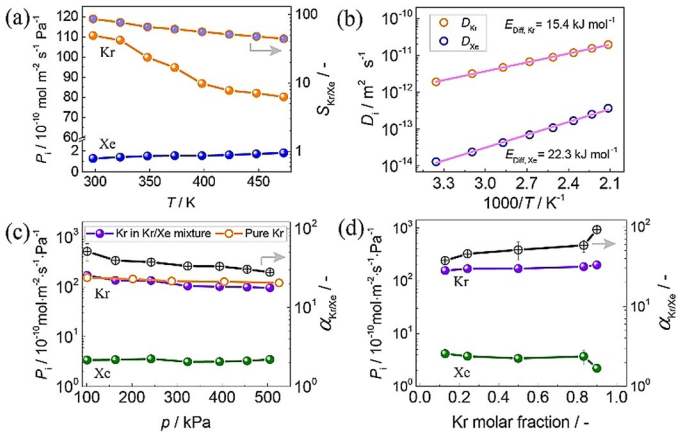

Figure 3. a,b) Single component permeation and diffusivity at different temperatures and 1.5 bara. c) Feed pressure-dependent Kr/Xe equimolar mixture separation performance at 298 K. d) Kr/Xe mixture separation performance for different compositions at 298 K and 1 bara. Membrane M2 was used.

fitted to a single-site Langmuir model (Figure 2). The Kr desorption branches overlap well with the adsorption ones while the ones of Xe show a slight hysteresis in the low pressure range, indicating some restricted Xe diffusion. High-silica CHA is more adsorption selective for Xe over Kr, evidenced by the higher adsorption heat of Xe over Kr (Figure S3a). This can be well explained by the confinement effect[29] and the stronger interaction[30] (thermodynamic control). An unfavorable (high) Xe-adsorption selectivity would compromise a Kr/Xe diffusion selectivity so that current polycrystalline membranes exhibit a low or moderate Kr/Xe selectivity (0.98–45, Table S1).[16,31] The Xe adsorption heat of high-silica CHA zeolite (20.4 kJ mol^{-1}) is 10% lower than the benchmark SAPO-34 (22.5 kJ mol^{-1}).[16a] Remarkably, both adsorption heats are fairly constant with loading, revealing a homogeneous structure and the effect of aluminum traces (Si/Al ratio > 50) on gas uptake can be ignored.[32] The ideal adsorbed solution theory (IAST) Xe/Kr adsorption selectivity is only half that of SAPO-34 (6.7 vs. 12.0, Figure S3b).[16a] Following this line, a smaller competitive adsorption effect would improve the high-silica CHA zeolite membrane performance.[33]

To get more insight in the separation mechanism, single gas permeation of CO_2, N_2, Kr, CH_4 and Xe was measured for membrane M2 (Figure 3a and Figure S4a) and described by a Maxwell-Stefan formulation.[15a,34] Together with the adsorption parameters derived from single-site Langmuir fitting (Table S2), the temperature-dependent diffusivity was estimated (Figure 3b). It must be emphasized that a loading-dependent diffusivity is not explicitly considered, and if present, is therefore contained in the diffusivity activation energy.[34] Here we demonstrate Kr atoms diffuse two orders of magnitude faster than Xe, and even molecular dynamic simulation reveals that diffusion selectivity dominates the overall membrane selectivity.[15a,35] The diffusion selectivity of Kr over Xe is up to 146 at 298 K for membrane M2, which is two-fold higher than for the benchmark SAPO-34 zeolite membranes (65.2).[16d] The ultrahigh selectivity can be explained by the stronger size-exclusion effect (molecular sieving) of high-silica CHA zeolite, benefiting from the smaller aperture (0.370 × 0.417 nm)[21,36] and more rigid framework.[23] Even though cation-exchange with K^+ increased the diffusion selectivity of SAPO-34 zeolite membranes by 63%, the Kr permeance was considerably low (6.3×10^{-9} mol m^{-2} s^{-1} Pa^{-1}).[16d] The single component Kr permeance of our high-silica CHA zeolite membrane gave 1.10×10^{-8} mol m^{-2} s^{-1} Pa^{-1} at 298 K and monotonically decreased with temperature up to 473 K. Considering the increasing diffusivity, the decreasing adsorbed amount dominates the Kr permeance.[37] In the case of Xe, a more restricted diffusion and a relatively high activation energy ($E_{diff,Kr} = 15.4$ kJ mol^{-1} and $E_{diff,Xe} = 22.3$ kJ mol^{-1}) is encountered due to the fact that the kinetic diameter is bigger than the elliptical window opening. The activation energy of Xe diffusion is even higher than the heat of adsorption (20.4 kJ mol^{-1}). This explains well the monotonic increase of Xe permeance and the decreased ideal selectivity of Kr over Xe with increasing temperature.[37]

To estimate the potential for practical application, we further evaluated the membrane performance in the separation of Kr/Xe mixtures. For an equimolar mixture, the Xe permeance increased with temperature while the Kr permeance was relatively constant, leading to a decreasing Kr/Xe selectivity from 51 at 298 K to 43 at 348 K (Figure S5), which is still three times higher than the benchmark SAPO-34 zeolite membranes at elevated temperature ($\alpha_{Kr/Xe} = 12$, Table S1).[16b] The high quality of our high-silica CHA zeolite membrane is further shown by the constant Xe permeance with pressure, indicating the absence of viscous flow (Figure 3c). The Kr permeance decreased with pressure, similarly as for the single component permeation, due to nonlinear adsorption.[38] Eventually the high-silica CHA zeolite membranes showed a Kr permeance of 1.0×10^{-8} mol m^{-2} s^{-1} Pa^{-1} and a Kr/Xe selectivity of 28 at 5 bara. The binary and single component Kr permeance are nearly the same, further proving our hypothesis of less competitive adsorption.

The performance of the high-silica CHA zeolite membranes reported here far surpasses the state-of-the-art polymeric membranes (Figure 4).[39] Compared with other poly-

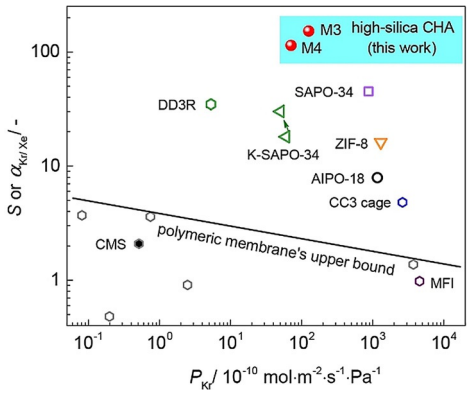

Figure 4. Comparison of high-silica CHA zeolite membrane performance in this work with other membranes, including SAPO-34,[16a–d] K-SAPO-34,[16d] AlPO-18,[16c] DD3R, ZIF-8,[16e] CC3 cage,[16f] carbon molecular sieve (CMS)[31] and MFI[31] (raw data points given in Table S1). The polymeric membrane's upper bound for Kr/Xe separation is taken from ref. [39].

crystalline membranes (including SAPO-34,[16a–d] K-SAPO-34,[16d] $AlPO_4$-18,[16c] DD3R, ZIF-8[16e] and CC3 cage[16f]), a maximum selectivity was achieved by high-silica CHA zeolite membranes. The ultrahigh selectivity was obtained over a wide range of feed compositions (Figure 3d and Table S3). Considering the lower presence of Kr over Xe encountered in the spent nuclear fuel reprocessing off-gas (9/91),[16a] a high selectivity is essential for less membrane stages and reducing the capital investment and operation cost.[40]

Although water vapor is typically present in the spent nuclear fuel reprocessing off-gas, its influence on the Kr/Xe separation performance and stability of the membranes has not been addressed yet.[16b,d,e] Here we evaluated the hydrothermal stability of high-silica CHA zeolite membranes for Kr/Xe separation under humid conditions (Figure 5a). In the dry binary mixture the Kr permeance was 1.2×10^{-8} mol m^{-2} s^{-1} Pa^{-1} with a Kr/Xe selectivity of 152. Both the Kr permeance and selectivity decreased once the feed was saturated with water vapor. However, Kr permeance gradually recovered when the humidified gas supply was stopped, reaching 87.5% initial performance after 6 h, benefiting from the hydrophobic nature of high-silica.[41] In contrast, the adsorbed water completely blocks the SAPO-34 channels,[17] and even worse, the framework collapses through dynamic hydrolysis of Si-O-Al and P-O-Al bonds.[18] The original permeance of high-silica CHA zeolite membrane was recovered by heating at 473 K for 12 h, indicating only physical water adsorption occurred in our high-silica CHA zeolite membrane.[15a] The membrane kept a constant performance after one more humid feed cycle of totally one week, confirming reliable stability of high-silica CHA zeolite membranes for moisture-saturated Kr/Xe separation.

The radioactive stability of high-silica CHA zeolite was confirmed by exposure to γ-radiation for 30 days. The irradiation dose used was 100 kGy, identical to the total dose coming from ^{85}Kr in off-gas for one year exposure.[39] Herein, we used BET area, micropore volume and X-ray power diffraction as indicators to track the framework integrity before and after irradiation. The BET area and micropore volume are essentially constant within less than 5% (Figure 5b). CHA zeolite without any impurity phase was identified from PXRD patterns (Figure 5c). In contrast, phase changes were observed for MOF SIFSIX-3 at 1 kGy[12a] and nickel formate was identified for MOF NiDOBDC at 67.2 kGy.[42] For current benchmark SAPO-34 zeolite membranes, the separation performance dropped by 36.6% over 60 days storage and irradiation under atmosphere conditions.[20] Therefore, high-silica CHA zeolite is considered the new benchmark polycrystalline membrane material for radioactive Kr separation from Xe.

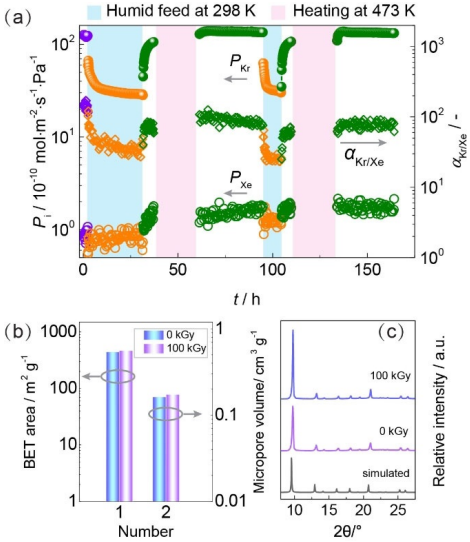

Figure 5. a) Hydrothermal stability of high-silica CHA zeolite membrane for dry (purple and green label) and humid (2.3 kPa water vapor, orange label) Kr/Xe mixture separation at 298 K. Membrane M3 was used. b,c) BET area, micropore volume and PXRD of high-silica CHA zeolite before and after γ-irradiation for 30 days and 100 kGy.

Conclusion

In summary, we demonstrated that high-silica CHA zeolite membranes possess ultra-high selectivity and irradiation stability for Kr/Xe separation. The Kr/Xe selectivity up to 152 surpasses the current polymeric and polycrystalline membranes, and the membrane exhibited stable performance in a moisture-saturated mixture for more than one week. Together with the superior irradiation stability (> 100 kGy), the high-silica CHA zeolite membrane paves the way for separating radioactive ^{85}Kr from Xe, reaching a notable decrease in the volatile nuclear waste storage volume.

Acknowledgements

This work is sponsored by the National Natural Science Foundation of China (21908097 and U1967215), Jiangsu Specially-Appointed Professors Program and "333 Talent Project" of Jiangsu Province, State Key Laboratory of Materials-Oriented Chemical Engineering (ZK202002).

Conflict of interest

The authors declare no conflict of interest.

Keywords: CHA zeolite · gas separation · krypton · membrane · xenon

[1] "Radioactive waste management", can be found under https://world-nuclear.org/information-library/nuclear-fuel-cycle/nuclear-wastes/radioactive-waste-management.aspx, accessed 2021-01-30.

[2] D. Sheng, L. Zhu, C. Xu, C. Xiao, Y. Wang, Y. Wang, L. Chen, J. Diwu, J. Chen, Z. Chai, T. E. Albrecht-Schmitt, S. Wang, *Environ. Sci. Technol.* **2017**, *51*, 3471 – 3479.

[3] a) A. Bollhöfer, C. Schlosser, S. Schmid, M. Konrad, R. Purtschert, R. Krais, *J. Environ. Radioact.* **2019**, *205 – 206*, 7 – 16; b) J. Ahlswede, S. Hebel, J. O. Ross, R. Schoetter, M. B. Kalinowski, *J. Environ. Radioact.* **2013**, *115*, 34 – 42.

[4] D. Butkus, J. Kleiza, *J. Radioanal. Nucl. Chem.* **2011**, *287*, 247 – 254.

[5] H. Yusa, M. Kikuchi, H. Tsuchiya, O. Kawaguchi, T. Segawa, *Nucl. Eng. Des.* **1977**, *41*, 437 – 441.

[6] S. U. Nandanwar, K. Coldsnow, A. Porter, P. Sabharwall, D. E. Aston, D. N. McIlroy, V. Utgikar, *Chem. Eng. J.* **2017**, *320*, 222 – 231.

[7] S. U. Nandanwar, K. Coldsnow, V. Utgikar, P. Sabharwall, D. E. Aston, Y. Zhang, *Adsorption* **2016**, *22*, 129 – 137.

[8] a) Y. Wang, W. Liu, Z. Bai, T. Zheng, M. A. Silver, Y. Li, Y. Wang, X. Wang, J. Diwu, Z. Chai, S. Wang, *Angew. Chem. Int. Ed.* **2018**, *57*, 5783 – 5787; *Angew. Chem.* **2018**, *130*, 5885 – 5889; b) Q. Wang, T. Ke, L. Yang, Z. Zhang, X. Cui, Z. Bao, Q. Ren, Q. Yang, H. Xing, *Angew. Chem. Int. Ed.* **2020**, *59*, 3423 – 3428; *Angew. Chem.* **2020**, *132*, 3451 – 3456; c) L. Li, L. Guo, Z. Zhang, Q. Yang, Y. Yang, Z. Bao, Q. Ren, J. Li, *J. Am. Chem. Soc.* **2019**, *141*, 9358 – 9364; d) G. Yu, Y. Liu, X. Zou, N. Zhao, H. Rong, G. Zhu, *J. Mater. Chem. A* **2018**, *6*, 11797 – 11803.

[9] a) J. Li, L. Huang, X. Zou, A. Zheng, H. Li, H. Rong, G. Zhu, *J. Mater. Chem. A* **2018**, *6*, 11163 – 11168; b) D. Chakraborty, S. Nandi, M. Sinnwell, J. Liu, R. Kushwaha, P. K. Thallapally, R. Vaidhyanathan, *ACS Appl. Mater. Interfaces* **2019**, *11*, 13279 – 13284.

[10] D. Banerjee, C. M. Simon, S. K. Elsaidi, M. Haranczyk, P. K. Thallapally, *Chem* **2018**, *4*, 466 – 494.

[11] a) C. A. Fernandez, J. Liu, P. K. Thallapally, D. M. Strachan, *J. Am. Chem. Soc.* **2012**, *134*, 9046 – 9049; b) C. M. Simon, R. Mercado, S. K. Schnell, B. Smit, M. Haranczyk, *Chem. Mater.* **2015**, *27*, 4459 – 4475.

[12] a) S. K. Elsaidi, M. H. Mohamed, A. S. Helal, M. Galanek, T. Pham, S. Suepaul, B. Space, D. Hopkinson, P. K. Thallapally, J. Li, *Nat. Commun.* **2020**, *11*, 3103; b) J. Liu, C. A. Fernandez, P. F. Martin, P. K. Thallapally, D. M. Strachan, *Ind. Eng. Chem. Res.* **2014**, *53*, 12893 – 12899.

[13] Y. Peng, Y. Li, Y. Ban, W. Yang, *Angew. Chem. Int. Ed.* **2017**, *56*, 9757 – 9761; *Angew. Chem.* **2017**, *129*, 9889 – 9893.

[14] Y. Huang, L. Wang, Z. Song, S. Li, M. Yu, *Angew. Chem. Int. Ed.* **2015**, *54*, 10843 – 10847; *Angew. Chem.* **2015**, *127*, 10993 – 10997.

[15] a) X. Wang, Y. Zhang, X. Wang, E. Andres-Garcia, P. Du, L. Giordano, L. Wang, Z. Hong, X. Gu, S. Murad, F. Kapteijn, *Angew. Chem. Int. Ed.* **2019**, *58*, 15518 – 15525; *Angew. Chem.* **2019**, *131*, 15664 – 15671; b) X. Wang, P. Karakiliç, X. Liu, M. Shan, A. Nijmeijer, L. Winnubst, J. Gascon, F. Kapteijn, *ACS Appl. Mater. Interfaces* **2018**, *10*, 33574 – 33580.

[16] a) X. Feng, Z. Zong, S. K. Elsaidi, J. B. Jasinski, R. Krishna, P. K. Thallapally, M. A. Carreon, *J. Am. Chem. Soc.* **2016**, *138*, 9791 – 9794; b) Y. Hye Kwon, C. Kiang, E. Benjamin, P. Crawford, S. Nair, R. Bhave, *AIChE J.* **2017**, *63*, 761 – 769; c) T. Wu, J. Lucero, Z. Zong, S. K. Elsaidi, P. K. Thallapally, M. A. Carreon, *ACS Appl. Nano Mater.* **2018**, *1*, 463 – 470; d) Y. H. Kwon, B. Min, S. Yang, D.-Y. Koh, R. R. Bhave, S. Nair, *ACS Appl. Mater. Interfaces* **2018**, *10*, 6361 – 6368; e) T. Wu, X. Feng, S. K. Elsaidi, P. K. Thallapally, M. A. Carreon, *Ind. Eng. Chem. Res.* **2017**, *56*, 1682 – 1686; f) J. M. Lucero, M. A. Carreon, *ACS Appl. Mater. Interfaces* **2020**, *12*, 32182 – 32188.

[17] J. C. Poshusta, R. D. Noble, J. L. Falconer, *J. Membr. Sci.* **2001**, *186*, 25 – 40.

[18] T. Sun, S. Xu, D. Xiao, Z. Liu, G. Li, A. Zheng, W. Liu, Z. Xu, Y. Cao, Q. Guo, N. Wang, Y. Wei, Z. Liu, *Angew. Chem. Int. Ed.* **2020**, *59*, 20672 – 20681; *Angew. Chem.* **2020**, *132*, 20853 – 20862.

[19] X. Liu, X. Wang, F. Kapteijn, *Chem. Rev.* **2020**, *120*, 8303 – 8377.

[20] S. Nair, "Zeolite membranes for krypton/xenon separation from spent nuclear fuel reprocessing off-gas", can be found under https://neup.inl.gov/SiteAssets/Final%20%20Reports/FY%202014/14-6309%20NEUP%20Final%20Report.pdf, accessed 2021-01-30.

[21] E. Kim, W. Cai, H. Baik, J. Choi, *Angew. Chem. Int. Ed.* **2013**, *52*, 5280 – 5284; *Angew. Chem.* **2013**, *125*, 5388 – 5392.

[22] P. Cnudde, R. Demuynck, S. Vandenbrande, M. Waroquier, G. Sastre, V. V. Speybroeck, *J. Am. Chem. Soc.* **2020**, *142*, 6007 – 6017.

[23] P. Ferri, C. Li, R. Millán, J. Martínez-Triguero, M. Moliner, M. Boronat, A. Corma, *Angew. Chem. Int. Ed.* **2020**, *59*, 19708 – 19715; *Angew. Chem.* **2020**, *132*, 19876 – 19883.

[24] L. Yu, A. Holmgren, M. Zhou, J. Hedlund, *J. Mater. Chem. A* **2018**, *6*, 6847 – 6853.

[25] a) L. Zhai, X. Yu, Y. Wang, J. Zhang, Y. Ying, Y. Cheng, S. B. Peh, G. Liu, X. Wang, Y. Cai, D. Zhao, *J. Membr. Sci.* **2020**, *610*, 118239; b) X. Wang, L. Zhai, Y. Wang, R. Li, X. Gu, Y. D. Yuan, Y. Qian, Z. Hu, D. Zhao, *ACS Appl. Mater. Interfaces* **2017**, *9*, 37848 – 37855.

[26] M. J. den Exter, H. van Bekkum, C. J. M. Rijn, F. Kapteijn, J. A. Moulijn, H. Schellevis, C. I. N. Beenakker, *Zeolites* **1997**, *19*, 13 – 20.

[27] M. Kumar, H. Luo, Y. Román-Leshkov, J. D. Rimer, *J. Am. Chem. Soc.* **2015**, *137*, 13007 – 13017.

[28] X. Wang, Z. Yang, C. Yu, L. Yin, C. Zhang, X. Gu, *Microporous Mesoporous Mater.* **2014**, *197*, 17 – 25.

[29] C. G. Saxton, A. Kruth, M. Castro, P. A. Wright, R. F. Howe, *Microporous Mesoporous Mater.* **2010**, *129*, 68 – 73.

[30] A. Monpezat, S. Topin, L. Deliere, D. Farrusseng, B. Coasne, *Ind. Eng. Chem. Res.* **2019**, *58*, 4560 – 4571.

[31] P. G. Crawford, *Zeolite membranes for the separation of krypton and xenon from spent nuclear fuel reprocessing off-gas*, Master Thesis, Georgia Institute of Technology **2013**.

[32] a) N. Kosinov, C. Auffret, C. Gucuyener, B. M. Szyja, J. Gascon, F. Kapteijn, E. J. M. Hensen, *J. Mater. Chem. A* **2014**, *2*, 13083 – 13092; b) P. Karakiliç, X. Wang, F. Kapteijn, A. Nijmeijer, L. Winnubst, *J. Membr. Sci.* **2019**, *586*, 34 – 43.

[33] K. V. Lawler, A. Sharma, B. Alagappan, P. M. Forster, *Microporous Mesoporous Mater.* **2016**, *222*, 104 – 112.

[34] J. van den Bergh, W. Zhu, J. Gascon, J. A. Moulijn, F. Kapteijn, *J. Membr. Sci.* **2008**, *316*, 35 – 45.

[35] a) R. Anderson, B. Schweitzer, T. Wu, M. A. Carreon, D. A. Gómez-Gualdrón, *ACS Appl. Mater. Interfaces* **2018**, *10*, 582 – 592; b) A. Hasanzadeh, J. Azamat, S. Pakdel, H. Erfan-Niya, A. Khataee, *Chem. Pap.* **2020**, https://doi.org/10.1007/s11696-020-01139-9.

[36] N. Hedin, G. J. DeMartin, W. J. Roth, K. G. Strohmaier, S. C. Reyes, *Microporous Mesoporous Mater.* **2008**, *109*, 327 – 334.

[37] F. Kapteijn, J. M. van de Graaf, J. A. Moulijn, *AIChE J.* **2000**, *46*, 1096 – 1100.

[38] J. M. van de Graaf, F. Kapteijn, J. A. Moulijn, *J. Membr. Sci.* **1998**, *144*, 87 – 104.

[39] S. Yu, S. Li, H. Wang, C. Zhu, J. Hou, S. Cui, X. Shen, Y. Liu, *J. Membr. Sci.* **2020**, *611*, 118280.
[40] X. Wang, M. Shan, X. Liu, M. Wang, C. M. Doherty, D. Osadchii, F. Kapteijn, *ACS Appl. Mater. Interfaces* **2019**, *11*, 20098 – 20103.
[41] a) M. Lee, S. Hong, D. Kim, E. Kim, K. Lim, J. C. Jung, H. Richter, J.-H. Moon, N. Choi, J. Nam, J. Choi, *ACS Appl. Mater. Interfaces* **2019**, *11*, 3946 – 3960; b) E. Jang, S. Hong, E. Kim, N. Choi, S. J. Cho, J. Choi, *J. Membr. Sci.* **2018**, *549*, 46 – 59.
[42] "Separations and waste forms research and development FY 2013 accomplishments report", can be found under https://www.osti.gov/servlets/purl/1123845, accessed 2021-01-30.

Manuscript received: January 7, 2021
Accepted manuscript online: February 2, 2021
Version of record online: March 8, 2021

